Shell-Model Study of Calcium Isotopic Chain Starting from Chiral Two- and Three-Body Potentials

L. Coraggio[a] and Y. Z. Ma[b]

[a] *Istituto Nazionale di Fisica Nucleare, Complesso Universitario di Monte S. Angelo, Via Cintia — I-80126 Napoli, Italy*

[b] *School of Physics and State Key Laboratory of Nuclear Physics and Technology, Peking University, Beijing I-100871, China*

Abstract

We have studied neutron-rich calcium isotopes in terms of the nuclear shell model employing a realistic effective interaction derived from realistic two- and three-body potentials built up within the chiral perturbation theory. We focus our attention on the shell-evolution properties of such an isotopic chain, namely on the excitation energy of yrast $J^\pi = 2^+$ states and two-neutron separation energies of even-A isotopes. The calculated results are in a good agreement with the available experimental data up to ^{56}Ca, but show different predictions for heavier nuclei when including or not the three-body potential. In this context, the $N = 40$ shell closure and the location of calcium dripline is also discussed.

Keywords: *Nuclear shell model; effective interactions; nuclear forces*

1 Introduction

Heavy calcium isotopes with mass number $A > 48$ are currently the subject of great experimental and theoretical interest. With an N/Z ratio > 1.4 they lie far from the stability valley and provide a good opportunity to explore the evolution of shell structure when approaching the neutron drip line [1, 2]. In this context, it should be mentioned that the question of the appearance of a shell closure at $N = 34$ traces back to the work of Beiner and coworkers within the framework of the energy density formalism [3]. A decade ago some shell-model (SM) calculations [4, 5] have revived this issue indicating the existence of a large shell gap at $N = 34$, employing the empirical SM Hamiltonian GXPF1A [5]. On the other hand, the results of other SM calculations, obtained with different SM Hamiltonians, did not exhibit any shell closure for ^{54}Ca [6,7]. As a matter of fact, a decrease of the experimental 2_1^+ excitation energy in ^{54}Ca with respect the one in ^{56}Ca was observed in 2013, that evidences a lack of the $N = 34$ shell closure [8].

Proceedings of the International Conference 'Nuclear Theory in the Supercomputing Era — 2018' (NTSE-2018), Daejeon, South Korea, October 29 – November 2, 2018, eds. A. M. Shirokov and A. I. Mazur. Pacific National University, Khabarovsk, Russia, 2019, p. 192.

http://www.ntse.khb.ru/files/uploads/2018/proceedings/Coraggio.pdf.

The contradictory theoretical predictions point to the crucial role played by the SM Hamiltonian, and the weakening of predictive power of an empirical procedure to derive them.

The realistic shell-model provides an approach that may overcome the ambiguity of fitting the SM single-particle (SP) energies and two-body matrix elements (TBME) to a chosen set of observables, namely deriving the effective Hamiltonian by way of the many-body perturbation theory and starting from a realistic nuclear potential [9, 10].

To this end, we have performed a perturbative expansion of a fp-shell effective Hamiltonian $H_{\rm eff}$, arresting the series at the third order, and starting from a realistic nuclear two-nucleon force (2NF) based on the chiral perturbation theory (ChPT) at next-to-next-to-next-to-leading order ($\mathrm{N^3LO}$) [11]. We also include in our $H_{\rm eff}$, aside the above two-body potential, a chiral $\mathrm{N^2LO}$ three-body potential [12] whose effects are considered at first-order in perturbation theory.

As mentioned before, we draw our attention to the shell evolution of calcium isotopes, as can be inferred form the behavior of the yrast $J^\pi = 2^+$ states and ground-state (g.s.) energies. In particular, we want also to stress the role played by three-nucleon forces (3NF) to tackle this issue, so we will report results obtained using realistic SM effective Hamiltonians that include or not 3NF contributions.

The relevance of 3NF for a successful SM description of the evolution of shell closures traces back to the seminal papers of Zuker and coworkers [13, 14], who have investigated the need of modifications of the monopole component of TBME obtained from realistic SM Hamiltonians [15]. They also inferred that this should trace back to the lack of a 3NF in the nuclear realistic potentials employed to derive the $H_{\rm eff}$ [16].

Extensive direct investigations about the role of 3NFs in realistic $H_{\rm eff}$ have been carried out more recently by Schwenk and coworkers, who have performed studies of calcium [17, 18] isotopic chain starting from nuclear potentials built up within the chiral perturbative expansion and softened by way of $V_{\rm low-k}$ technique [19] or the similarity renormalization-group (SRG) approach [20].

This paper is organized as follows. First, a brief description of the derivation of $H_{\rm eff}$ within the perturbative approach is reported in Section 2. Section 3 is devoted to the presentation of the results of our calculations of the excitation energy $E^{\rm exc}_{2^+}$ of the yrast $J^\pi = 2^+$ states and two-neutron separation energies S_{2n} for the calcium isotopes ranging from $N = 22$ to $N = 42$, and compare them with the available data from experiment. In Section 4 we discuss our results and make some concluding remarks.

2 Outline of calculations

As mentioned before, we consider as 2NF the chiral $\mathrm{N^3LO}$ potential derived by Entem and Machleidt in Ref. [11], and as 3NF a chiral $\mathrm{N^2LO}$ potential, which shares the regulator function of a nonlocal form and some of the low-energy constants (LECs) with the 2NF. It should be stressed that the $\mathrm{N^2LO}$ 3NF is composed of three components, namely the two-pion (2π) exchange term $V_{3N}^{(2\pi)}$, the one-pion (1π) exchange plus contact term $V_{3N}^{(1\pi)}$, and the contact term $V_{3N}^{(\rm ct)}$, and, consistently, the LECs c_1, c_3, and c_4 appearing in $V_{\rm 3NF}^{(2\pi)}$, are the same as those in the $\mathrm{N^3LO}$ 2NF.

Besides this, the 3NF 1π-exchange and contact terms are own two extra LECs (known as c_D and c_E, respectively), which need to be determined by reproducing observables in systems with mass $A > 2$.

For our calculations, we adopt the same c_D and c_E values as employed in Ref. [21], namely, $c_D = -1$ and $c_E = -0.34$, that have been determined by way of no-core shell model (NCSM) calculations [12].

The details about the calculation of our 3NF matrix elements in the harmonic-oscillator (HO) basis can be found in Appendix of Ref. [21]. The Coulomb potential is explicitly taken into account in our calculations.

In Ref. [21], it can be found also a detailed description of the derivation of our $H_{\rm eff}$ for one- and two-valence nucleon systems, starting from 2NF and 3NF, while here we present only a brief summary.

Our $H_{\rm eff}$ are derived in the model space spanned by the five orbitals, $0f_{7/2}$, $0f_{7/2}$, $1p_{3/2}$, $1p_{1/2}$, $0g_{9/2}$, outside the doubly-closed ^{40}Ca. We have added the $0g_{9/2}$ orbital to the standard fp ones in order to have a sounder description of neutron-rich systems and to investigate the location of neutron dripline in calcium isotopes.

We introduce an auxiliary one-body potential U to break up the Hamiltonian H for a system of A nucleons into a sum of a one-body term H_0, which describes the independent motion of the nucleons, and a residual interaction H_1:

$$H = \sum_{i=1}^{A} \frac{p_i^2}{2m} + \sum_{i<j=1}^{A} V_{ij}^{\rm 2NF} + \sum_{i<j<k=1}^{A} V_{ijk}^{\rm 3NF} = T + V^{\rm 2NF} + V^{\rm 3NF}$$
$$= (T+U) + (V^{\rm 2NF} - U) + V^{\rm 3NF} = H_0 + H_1^{\rm 2NF} + H_1^{\rm 3NF}. \quad (1)$$

In our calculation we use the HO potential, $U = \frac{1}{2}m\omega^2 r^2$, with the oscillator parameter $\hbar\omega = 11$ MeV, according to the expression $\hbar\omega = 45A^{-1/3} - 25A^{-2/3}$ for $A = 40$.

Once the H_0 has been introduced, the reduced model space is defined in terms of a finite subset of H_0's eigenvectors. The diagonalization of the many-body Hamiltonian in Eq. (1) within the infinite Hilbert space is then reduced to the solution of an eigenvalue problem for an effective Hamiltonian $H_{\rm eff}$ in a finite space.

We employ the time-dependent perturbation theory to derive $H_{\rm eff}$ [10,22]. $H_{\rm eff}$ is expressed through the Kuo–Lee–Ratcliff folded-diagram expansion in terms of the vertex function $\hat{Q}$-box, which is composed of irreducible valence-linked diagrams [23,24]. We include in the $\hat{Q}$-box one- and two-body Goldstone diagrams through the third order in $H_1^{\rm 2NF}$ and up to the first order in $H_1^{\rm 3NF}$. It is worth pointing out that the input chiral 2NF and 3NF have not been modified by way of any renormalization procedure, and the perturbative properties of the $\hat{Q}$-box from N^{3}LO 2NF potential have been discussed in Ref. [22]. The folded-diagram series is then summed up to all orders using the Lee–Suzuki iteration method [25].

The $H_{\rm eff}$ derived for one valence-nucleon systems contains only one-body contributions which provides the SP energies for the SM calculation, while the two-body matrix elements are obtained from $H_{\rm eff}$ derived from the two valence-nucleon systems once the theoretical SP energies are subtracted from its diagonal matrix elements.

We have derived two $H_{\rm eff}$; one has been obtained calculating $\hat{Q}$-box diagrams with 2NF vertices only, and the other has been built up including also $H_1^{\rm 3NF}$ first-order contributions in the collection of $\hat{Q}$-box diagrams (see Fig. 3 in Ref. [21]).

The neutron SP energies calculated with respect to $0f_{7/2}$ orbital are reported in Table 1.

We observe that the $\epsilon_{p_{3/2}} - \epsilon_{f_{7/2}}$ splitting provided by the 2NF only is too small to secure the shell closure of ^{48}Ca, so, when diagonalizing the SM Hamiltonians, we

Table 1: Theoretical neutron SP energies (in MeV) derived starting from 2NF only (first column), and including 3NF contributions too (second column).

orbital	$\epsilon_\nu^{\rm 2NF}$	$\epsilon_\nu^{\rm 2NF+3NF}$
$0f_{7/2}$	0.0	0.0
$0f_{5/2}$	4.6	5.8
$1p_{3/2}$	0.6	2.8
$1p_{1/2}$	2.0	4.3
$0g_{9/2}$	1.9	6.7

consider the same set of SP energies, namely, the one calculated including also the 3NF contributions. We dub the $H_{\rm eff}$ with TBME derived with the 2NF only $H_{\rm eff}^{\rm 2NF}$, and $H_{\rm eff}^{\rm 3NF}$ is the one whose SP energies and TBME have been obtained by adding also the 3NF.

3 Results

We start our study of calcium isotopes showing in Fig. 1 our results of their $E_{2^+}^{\rm exc}$ from $N = 22$ up to $N = 42$ (blue triangles and black diamonds), and compare them with available experimental data [8, 26] (red dots).

We observe that the behaviors obtained with both $H_{\rm eff}$ are very similar up to $N = 38$, the results with $H_{\rm eff}^{\rm 3NF}$ are in a better agreement with experiment. The shell closure at $N = 28$ is reproduced, as well as the subshell closure at $N = 32$ and the slight excitation-energy decrease between $N = 32$ and $N = 34$.

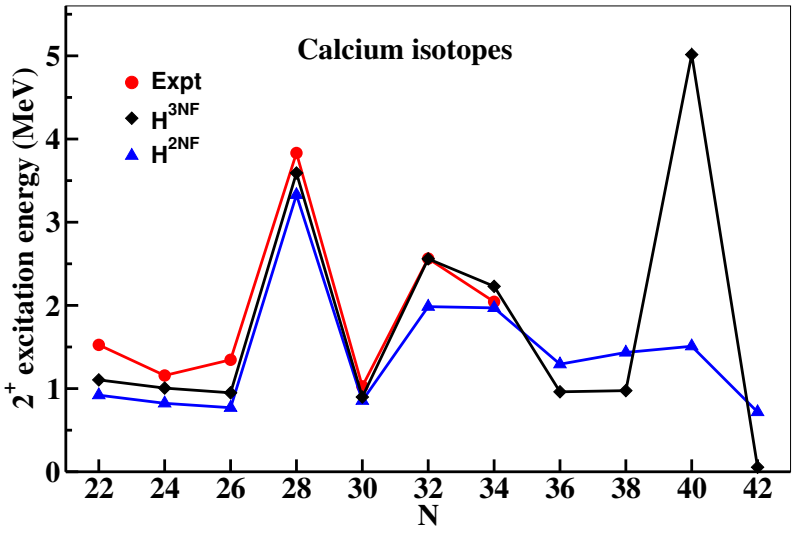

Figure 1: Experimental (red dots) and calculated excitation energies of the yrast $J^\pi = 2^+$ states for calcium isotopes from $N = 22$ to 42. The results obtained with $H_{\rm eff}^{\rm 2NF}$ are reported with blue triangles, those with $H_{\rm eff}^{\rm 3NF}$ are drawn as black diamonds.

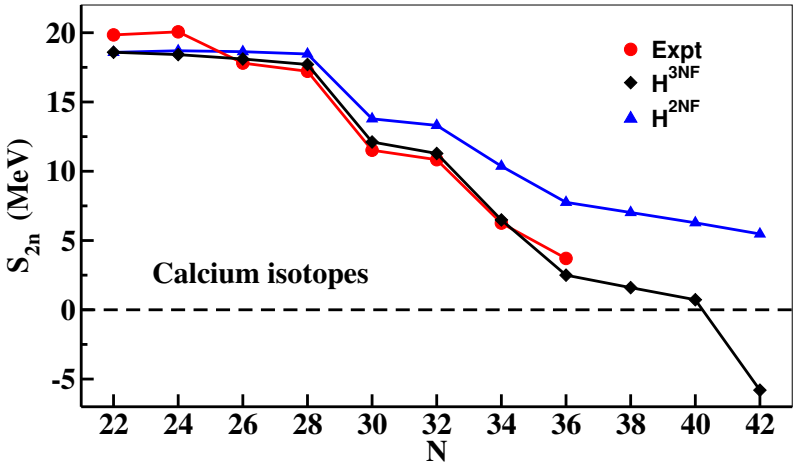

Figure 2: Experimental and calculated two-neutron separation energies for calcium isotopes from $N = 22$ to 42. See text for details.

The comparison with the data for lighter isotopes are less satisfactory, these systems are largely affected by core-excitation components of ^{40}Ca that have not been taken explicitly into account.

The larger discrepancy between the results obtained with $H_{\rm eff}^{\rm 2NF}$ and $H_{\rm eff}^{\rm 3NF}$ appears at $N = 40$, where the latter exhibits a strong closure of the $0f_{5/2}$ orbital. Since both Hamiltonians share the same set of SP energies, this feature traces back to different monopole component of the $0f_{5/2}, 0g_{9/2}$ configuration. In particular, this monopole component of $H_{\rm eff}^{\rm 3NF}$ enhances the energy splitting between the effective single-particle energies [27] of $0f_{5/2}$ and $0g_{9/2}$ orbitals when increasing the valence-neutron number, generating a strong shell closure at $N = 40$.

These closure properties are also present in the calculation of the two-neutron separation energies that are shown in Fig. 2 for the calcium isotopes up to $N = 42$. As before, the results obtained with $H_{\rm eff}^{\rm 2NF}$ are reported as blue triangle, while the $H_{\rm eff}^{\rm 3NF}$ ones are drawn as black diamonds. Data from experiment [1, 2, 28] are reported with red dots. It should be pointed out that we have shifted the SP energies in Table 1 in order to reproduce the experimental g.s. energy of ^{41}Ca [28].

We have reported the results up to $N = 42$ since $H^{\rm 3NF}$ predicts ^{60}Ca as the last bound isotope.

As can be seen, both experimental and theoretical S_{2n} show a rather flat behavior up to $N = 28$, then a sudden drop occurs at $N = 30$ that is a signature of the shell closure due to the $0f_{7/2}$ filling. Another decrease appears at $N = 34$ because at that point the valence neutrons start to occupy the $1p_{1/2}$ and $0f_{5/2}$ orbitals.

The results obtained with $H_{\rm eff}^{\rm 3NF}$ follow closely the behavior of the experimental S_{2n}, while those obtained with $H_{\rm eff}^{\rm 2NF}$ provide a less satisfactory agreement from $N = 28$ on. This supports the crucial role of 3NF contributions to reproduce the observed shell evolution.

As in the case of the calculated $E_{2^+}^{\rm exc}$, the difference obtained with $H_{\rm eff}^{\rm 2NF}$ and $H_{\rm eff}^{\rm 3NF}$ between the monopole component of $0f_{5/2}, 0g_{9/2}$ configuration is responsible for different slopes towards different neutron driplines. As a matter of fact, $H_{\rm eff}^{\rm 2NF}$ pro-

vides bound calcium isotopes up to $N = 50$, while according to the SM calculations with $H_{\rm eff}^{\rm 3NF}$ the calcium dripline should be located at ^{60}Ca.

4 Concluding remarks

We have presented the results of SM calculations for the calcium isotopic chain, which have been performed employing the SM effective Hamiltonian derived from realistic two- and three-body potentials built up within the chiral perturbation theory.

The outcome of our calculation is manifold.

a) Single-particle energies obtained from the effective SM Hamiltonian starting from the 2NF are not able to provide satisfactory shell-closure properties, especially the one at $N = 28$.

b) The 3NF contributions to the SP energies are crucial to reproduce the ^{48}Ca shell closure corresponding to the filling of the $0f_{7/2}$ orbital.

c) The monopole component associated with the two-body matrix elements are rather different when including or not the 3NF. In particular, when adding the three-body potential to the starting Hamiltonian, we predict a strong shell closure at $N = 40$. This is at variance with the case when the effects of the three-body potential are neglected.

d) The difference observed in the monopole component of the $0f_{5/2}, 0g_{9/2}$ configuration leads to different predictions for the dripline, which is located at $N = 40$ when including the contributions of the three-body potential.

The last mentioned feature is quite intriguing, since the recent experimental observation of ^{60}Ca [29] and a study of the calcium isotopes by way of a Bayesian model averaging analysis [30] have revived the issue of the calcium dripline location.

References

[1] F. Wienholtz *et al.*, Nature **498**, 346 (2013).

[2] S. Michimasa *et al.*, Phys. Rev. Lett. **121**, 022506 (2018).

[3] M. Beiner, R. J. Lombard and D. Mas, Nucl. Phys. A **249**, 1 (1975).

[4] M. Honma, T. Otsuka, B. A. Brown and T. Mizusaki, Phys. Rev. C **69**, 034335 (2004).

[5] M. Honma, T. Otsuka, B. A. Brown and T. Mizusaki, Eur. Phys. J. A **25**, 499 (2005).

[6] A. Poves, J. Sánchez-Solano, E. Caurier, F. Nowacki, Nucl. Phys. A **694**, 157 (2001).

[7] E. Caurier, G. Martínez-Pinedo, F. Nowacki, A. Poves, A. P. Zuker, Rev. Mod. Phys. **77**, 427 (2005).

[8] D. Steppenbeck *et al.*, Nature **502**, 207 (2013).

[9] B. H. Brandow, Rev. Mod. Phys. **39**, 771 (1967).

[10] T. T. S. Kuo and E. Osnes, Lecture Notes Phys. **364**, 1 (1990).

[11] D. R. Entem and R. Machleidt, Phys. Rev. C **66**, 014002 (2002).

[12] P. Navrátil, V. G. Gueorguiev, J. P. Vary, W. E. Ormand and A. Nogga, Phys. Rev. Lett. **99**, 042501 (2007).

[13] E. Caurier, E. A. P. Zuker, A. Poves and G. Martínez-Pinedo, Phys. Rev. C **50**, 225 (1994).

[14] J. Duflo and A. P. Zuker, Phys. Rev. C **59**, 2347 (1999).

[15] T. T. S. Kuo and G. E. Brown, Nucl. Phys. **84**, 40 (1966).

[16] A. P. Zuker, Phys. Rev. Lett. **90**, 042502 (2003).

[17] J. D. Holt, T. Otsuka, A. Schwenk and T. Suzuki, J. Phys. G **39**, 085111 (2012).

[18] J. D. Holt, J. Menéndez, J. Simonis and A. Schwenk, Phys. Rev. C **90**, 024312 (2014).

[19] S. Bogner. T. T. S. Kuo, L. Coraggio, A. Covello and N. Itaco, Phys. Rev. C **65**, 051301 (2002).

[20] S. K. Bogner, R. J. Furnstahl and R. J. Perry, Phys. Rev. C **75**, 061001 (2007).

[21] T. Fukui, L. De Angelis, Y. Z. Ma, L. Coraggio, A. Gargano, N. Itaco and F. R. Xu, Phys. Rev. C **98**, 044305 (2018).

[22] L. Coraggio, A. Covello, A. Gargano, N. Itaco and T. T. S. Kuo, Ann. Phys. (NY) **327**, 2125 (2012).

[23] T. T. S. Kuo, S. Y. Lee and K. F. Ratcliff, Nucl. Phys. A **176**, 65 (1971).

[24] T. T. S. Kuo, J. Shurpin, K. C. Tam, E. Osnes and P. J. Ellis, Ann. Phys. (NY) **132**, 237 (1981).

[25] K. Suzuki and S. Y. Lee, Prog. Theor. Phys. **64**, 2091 (1980).

[26] http://www.nndc.bnl.gov/ensdf/.

[27] Y. Utsuno, T. Otsuka, T. Mizusaki and M. Honma, Phys. Rev. C **60**, 054315 (1999).

[28] G. Audi, A. H. Wapstra and C. Thibault, Nucl. Phys. A **729**, 337 (2003).

[29] O. B. Tarasov *et al.*, Phys. Rev. Lett. **121**, 022501 (2018).

[30] L. Neufcort, Y. C. Cao, W. Nazarewicz, E. Olsen and F. Viens, Phys. Rev. Lett. **122**, 062502 (2019).